Vibrational spectroscopy of articular cartilage

Lassi Rieppo, Juha Töyräs & Simo Saarakkala

Taylor & Francis
Taylor & Francis Group

Vibrational spectroscopy of articular cartilage

Lassi Rieppo[a,b], Juha Töyräs[b,c], and Simo Saarakkala[a,d,e]

[a]Research Unit of Medical Imaging, Physics and Technology, Faculty of Medicine, University of Oulu, Oulu, Finland; [b]Department of Applied Physics, University of Eastern Finland, Kuopio, Finland; [c]Diagnostic Imaging Center, Kuopio University Hospital, Kuopio, Finland; [d]Medical Research Center, University of Oulu and Oulu University Hospital, Oulu, Finland; [e]Department of Diagnostic Radiology, Oulu University Hospital, Oulu, Finland

ABSTRACT

Articular cartilage is a connective tissue that is located at the ends of long bones. Type II collagen, proteoglycans, water, and chondrocytes are the main constituents of articular cartilage. Osteoarthritis, the most common joint disease in the world, causes degenerative changes in articular cartilage tissue. Fourier transform infrared, Raman, and near infrared spectroscopic techniques offer versatile tools to assess biochemical composition and quality of articular cartilage. These vibrational spectroscopic techniques can be used to broaden our understanding about the compositional changes during osteoarthritis, and they also hold promise in disease diagnostics. In this article, the current literature of articular cartilage spectroscopic studies is reviewed.

Introduction

Articular cartilage (AC) is a tissue that covers the ends of articulating bones, e.g., femur and tibia in the knee joint. Its main functions are to redistribute the stresses applied to bone ends and, together with synovial fluid, to provide near frictionless surface between the bones (1). AC is mainly composed of type II collagen, proteoglycans, water, and cartilage cells, i.e., chondrocytes (2). Collagen forms a fibrillary network that has a highly organized structure. AC can be divided into three layers according to the orientation of collagen fibrils. In the superficial layer of AC, collagen fibrils are aligned parallel to the AC surface. In the transitional layer, the orientation is random as the fibril orientation gradually changes from parallel to the surface to perpendicular orientation. In the deep layer, the orientation is perpendicular to the AC surface (3). In addition, the calcified cartilage, where cartilage attaches to the subchondral bone, forms another distinct region in the cartilage.

Tissue composition and structure have an important role in biomechanical behavior of AC. The negatively charged glycosaminoglycan side chains of proteoglycans attract free ions and water into the tissue. On the other hand, the collagen network limits the volume of other

components inside the tissue. Proteoglycans are mainly responsible for the compressive properties of AC (4), while the collagen network determines the tensile stiffness of AC (5). AC constituents are inhomogeneously distributed throughout the tissue depth. The concentration of proteoglycans is low in the superficial layer of AC, and it increases towards the cartilage–bone junction (6, 7). The superficial layer is rich of collagen. The amount of collagen is smaller in the transitional layer, but increases again to its highest level at the deep layer (6).

Osteoarthritis (OA) is the most common joint disease in the world. The causes of primary OA are largely unknown, although certain risk factors, such as age, overweight, and injury, are known (2). Degenerative changes occur in AC tissue during OA. Typically, the first changes are seen in the superficial layer of AC: the amount of proteoglycans decreases (8) and fibrillation of the collagen network occurs (9). AC has a limited intrinsic capability of healing injuries. However, smaller injuries can be healed using surgical techniques (10). In the later stages of OA, the AC tissue may be completely worn out, which leads to joint arthroplasty being the only remaining treatment option.

Vibrational spectroscopic techniques, i.e., Fourier transform infrared (FTIR), Raman and near infrared (NIR) spectroscopies, offer excellent tools for AC research. FTIR and Raman spectroscopic imaging techniques offer high molecular specificity, and they can be used for imaging the biochemical composition of histological AC tissue sections. On the other hand, Raman and NIR spectroscopies can be applied to tissue samples without any sample processing. NIR spectroscopy offers a superior penetration depth in the tissue, whereas its molecular specificity is lower than in FTIR and Raman spectroscopies. Further, all of these techniques can be conducted using fiber optic probes, e.g., during arthroscopy to estimate the properties of AC tissue. The combination of these techniques enables versatile assessment of quantitative and qualitative features of AC.

FTIR spectroscopy (400–4,000 cm^{-1})

The term FTIR spectroscopy is often used when referring to mid-infrared (mid-IR) region spectroscopy, although FTIR spectrometers are available also for far and near infrared regions. In this article, FTIR refers to mid-IR region. In FTIR spectroscopy, the transmission of mid-IR light through the sample (or the reflection from the sample in some cases) is measured as a function of frequency. In a modern FTIR spectrometer, a broadband light source is used, and light interference is exploited to record absorption of light at different frequencies. It is possible to image areas from histological sections by combining an FTIR spectrometer with an optical microscope. This technique is commonly called FTIR imaging or FTIR microspectroscopy. Standard FTIR microscopes that utilize globar infrared light sources can collect chemical microscopic images with a spatial resolution of approximately 5–10 μm (11).

FTIR microspectroscopy can be conducted using either cryosectioned or paraffin-embedded sections. Typically, the thickness of the AC tissue sections for FTIR microspectroscopy is between 3 and 15 μm. Subsequently, the sections are placed onto infrared transparent windows, made, e.g., of BaF$_2$, ZnSe, or CaF$_2$. Recently, low-emissivity (low-e) slides have gained some popularity in FTIR imaging measurements of histological sections. The main advantage of low-e slides over salt windows, such as BaF$_2$, is their low price. Low-e slides are used in transflection mode, i.e., the signal passes through the section twice as it is reflected back from the slide. A comparison between transflectance and transmittance modes in bone,
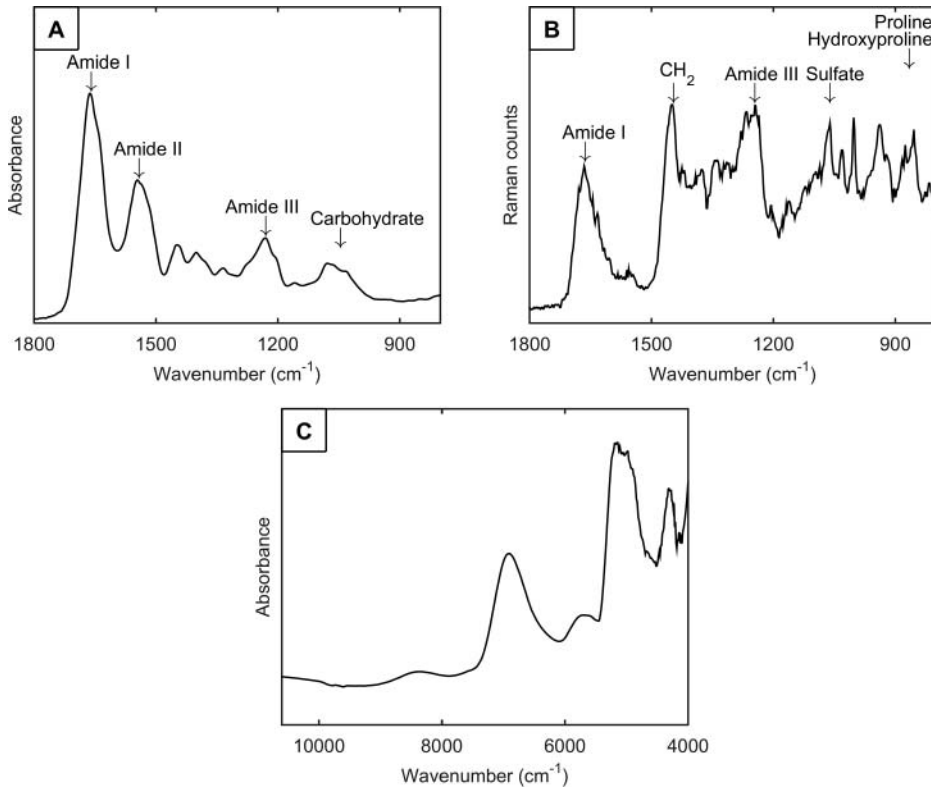
Figure 1. (A) FTIR spectrum, (B) Raman spectrum, and (C) NIR spectrum of articular cartilage. The assignments of the peaks seen in the spectra are listed in Tables 1 and 2.

tendon, and cartilage showed differences in peak shapes, positions, and intensities (12). These differences are likely due to distortions caused by the electric-field standing wave observed in transflectance measurements (13).

Cryosections are better than fixated samples in the sense that they are not chemically altered. However, in practice, they are more difficult to store and handle. It has been shown that the spectrum of fresh cartilage sample displays an altered amide I (1,590–1,720 cm^{-1}) /amide II (1,480–1,590 cm^{-1}) peak ratio after 24 h, which is an indication of degradation of the AC tissue (14). Paraffin-embedded samples require chemical fixation, which alters the chemical state of the sample. Paraffin is often removed from the section with, e.g., xylene, but it is difficult to achieve a complete removal of paraffin from the tissue (15). Another option is to leave paraffin in the section and subtract the paraffin spectrum from the tissue spectra after the measurements (16). Both cryosections (17) and paraffin-embedded tissue sections (18) have been shown to display noticeable variation in their thicknesses from the nominal section thickness cut with a cryotome or a microtome. Therefore, if peak heights are directly compared between the samples, it is recommended that more than one section per sample is measured and the average of the results is used to reduce the error caused by variable section thickness. Figure 1(A) shows a typical FTIR spectrum of AC. The origins of FTIR absorption peaks have been characterized for biological tissues. Some uncertainty exists in cases when peaks overlap with each other.

Table 1. Assignments of NIR (80, 84) and FTIR (19, 39, 50) peaks. Accessing individual peaks may require either curve fitting or the use of 2nd derivative spectra.

Wavenumber (cm^{-1})	Assignment
NIR	
8,820–8,060	C—H stretching (2nd overtone)
8,695–8,197	C—H stretching (2nd overtone)
7,460–6,780	O—H stretching (1st overtone)
7,280–6,040	O—H stretching (1st overtone)
6,890	Free water
5,720–5,500	C—H stretching (1st overtone)
5,200	Bound and free water
FTIR	
3,330	Amide A (N=H stretching)
1,720–1,580	Amide I region (C=O stretching)
1,690	Immature collagen cross-links
1,660	Mature collagen cross-links
1,580–1,490	Amide II region (C—N stretching, N—H bending, C—C stretching)
1,376	CH$_3$ bending of glycosaminoglycans
1,338	Collagen integrity (CH$_2$ side chain vibrations)
1,300–1,200	Amide III region (C—N stretching, N—H bending)
1,245	Sulfate asymmetric stretching
1,125–920	C—O—C, C—OH, C—C ring vibrations
1,062	Sulfate symmetric stretching
850	C—O—S stretching

Therefore, the peak assignments should only be regarded as suggestive. A list of possible peak assignments in AC is shown in Table 1.

The studies by Camacho et al. and Potter et al. set the groundwork for AC FTIR imaging research (19, 20). Camacho et al. developed univariate parameters for quantification of the collagen and proteoglycan contents in AC. The amide I (1,584–1,720 cm^{-1}) was shown to correlate with the amount of collagen and the carbohydrate region (984–1,140 cm^{-1}) correlated with the amount of aggrecan in pure compound mixtures of these components (19). A following study suggested that proteoglycan quantification could be improved by normalizing the carbohydrate region by the amide I in tissue-engineered cartilage by reducing the thickness variation in the sections (21). A statistically significant correlation was found between this ratio parameter and Alcian blue staining, which stains glycosaminoglycans (21). Later, a statistically significant correlation was shown also between the integrated area of the sulfate peak at 850 cm^{-1} and the DMMB staining for glycosaminoglycans (22). A qualitative parameter for evaluating the collagen integrity has also been developed. The study showed that the ratio of the integrated absorbances of the peak centered at 1,338 cm^{-1} and the amide II decreases as collagen of AC is degraded using collagenase enzyme. The peak at 1,338 cm^{-1} arises from the CH$_2$ side chain vibrations and is sensitive to the triple helical structure of type II collagen. Therefore, the peak ratio can be used to assess the collagen integrity (23).

Approach taken by Potter et al. was based on decomposing the measured cartilage FTIR spectra by utilizing pure compound spectra of tissue constituents. To assess the similarity between the spectra, the Euclidean distances between a measured cartilage spectrum and pure compound spectra are calculated. This gives information about the relative concentrations of the used pure compounds in the tissue (20). Alternatively, the linear combination of pure compound spectra can be used to decompose cartilage spectrum into components. In two studies, type II collagen and chondroitin sulfate were used as pure compounds in the linear combination model (20, 24). The tissue-engineered cartilage was found to contain more collagen and less
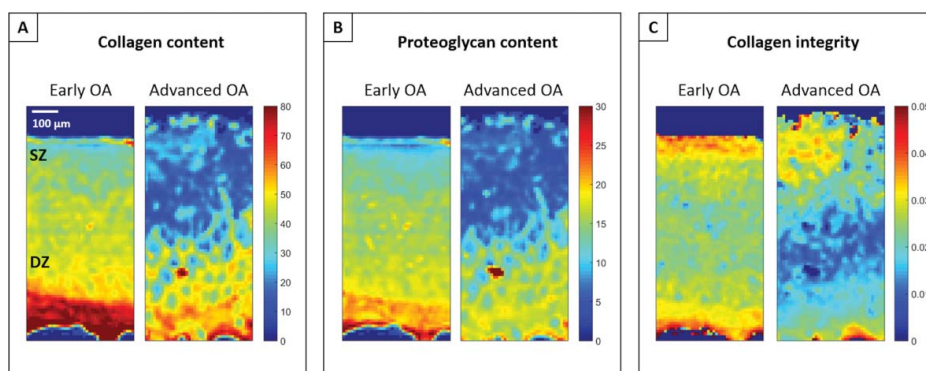
Figure 2. (A) Collagen content (the integrated absorbance of the amide I [1,585–1,720 cm^{-1}]), (B) proteoglycan content (the integrated absorbance of the carbohydrate region [984–1,140 cm^{-1}]), and (C) the collagen integrity (the ratio of the absorbance centered at 1,338 cm^{-1} to the amide II) from early OA and advanced OA tibial plateau samples obtained from total knee arthroplasty patients. In the figures, the full thickness of AC from superficial zone (SZ) to deep zone (DZ) is shown. Decrease in the collagen and the proteoglycan contents can be seen as the OA advances. In addition, significant changes in the collagen integrity are seen throughout the tissue depth.

proteoglycans than the native cartilage (20) and focal degenerative lesions in human osteoarthritic AC contained less proteoglycans than the surrounding healthy tissue (24).

The univariate methods are easy to implement, and, therefore, they have been applied in many studies (25–32). Collagen and proteoglycan concentration and collagen integrity maps produced using the univariate parameters in human tibial AC are shown in Figure 2. However, the molecular specificity of the univariate parameters for collagen and proteoglycans in human AC has been questioned because of the overlap between the absorption peaks (33). Enzymatic removal of proteoglycans can be used before conducting the measurements to increase the specificity of amide I parameter for collagen (34–36).

Vibrations from both proteoglycans and collagen exist in the carbohydrate region, even though it has been used directly for proteoglycan analysis. For this reason, alternative approaches have been explored. Two-dimensional correlation spectroscopy has been suggested to enhance the separation between the collagen and proteoglycans when analyzing the concentration gradients in AC (37). Curve fitting-derived sulfate peak at 1,060 cm^{-1} displayed better correlation with the optical density of safranin O than the integrated absorbance of the carbohydrate region when the depth-dependent distribution of proteoglycans was studied (38). Similar results were obtained by calculating the intensity of the sulfate peak from the 2nd derivative spectra (39). The sulfate peak also showed more consistent results than the integrated area of the carbohydrate region when two different species, human and bovine, were analyzed together (40).

Enzymatic removal of proteoglycans was used to evaluate the contribution of collagen and proteoglycans to absorbance and 2nd derivative spectra of bovine cartilage. As expected, the most significant changes in the raw spectra occurred in the carbohydrate region. Two 2nd derivative peaks, located at 1,062 cm^{-1} and 1,374 cm^{-1}, were assigned to proteoglycans, as they displayed the most significant reduction in their intensities due to the enzyme treatment. Multiple 2nd derivative peaks (1,202 cm^{-1}, 1,336 cm^{-1},

$1{,}448$ cm^{-1}, $1{,}514$ cm^{-1}, and $1{,}638$ cm^{-1}) displayed little or no changes in their intensities and, therefore, were classified as collagen-specific peaks (39).

The relative collagen and proteoglycan contents in bovine nasal cartilage were predicted by building a principal component regression (PCR) model using mixtures of collagen and chondroitin sulfate. Biochemical analysis was also performed for cartilage samples in order to confirm these results (41). Later, the same PCR model was applied to canine AC to examine depth-dependent concentration profiles of collagen and proteoglycans in AC (42). Furthermore, the differences in the proteoglycan content between healthy and osteoarthritic canine tibial AC were investigated using the earlier model. Proteoglycan loss in the meniscus-covered area of cartilage was found to be less than that of the meniscus-uncovered area (43). In another study, partial least squares (PLS) regression models were built to predict proteoglycan and collagen contents in bovine cartilage by calibrating the models against the optical density of safranin O or uronic acid content and hydroxyproline content for proteoglycans and collagen, respectively (44, 45). In addition, a PLS regression model for detecting the relative amounts of type I and type II collagens was built using pure compound mixtures. The model was shown to give reliable results in bone, tendon, normal and repair cartilage, and meniscus (46). The relationship between the FTIR spectra of bovine AC and its compressive stiffness was studied using PLS regression models combined with genetic algorithm for variable selection. Young's modulus and dynamic modulus were predicted from average spectra of the sample sections. High correlation between the FTIR data and the biomechanical parameters were achieved even though the models were based on the average spectra of the samples, i.e., the distributions of collagen and proteoglycans were not taken into account (47).

The peak area ratio of $1{,}660/1{,}690$ cm^{-1} has been commonly used to measure the cross-link maturity in type I collagen in bone (48). The peaks are found under the amide I band using curve fitting. The cross-link maturity has also been used to characterize a cartilage-like engineered biomass (49), and the maturity of cross-links of repair tissue in rabbit AC after full-thickness osteochondral defects. The maturity was initially greater in the repair tissue before reaching the levels present in the control tissue (50). However, the latter result was inconsistent with biochemical analyses. In human tibial plateau AC, the collagen maturity was shown to decrease significantly as a function of modified Mankin score (51).

Cluster analysis is a method that classifies spectra based on the similarities between the spectra. The use of cluster analysis was first demonstrated in murine AC, where hierarchical cluster analysis (HCA) separated a chondrocyte-rich layer in the superficial layer of cartilage from the rest of the tissue (52, 53). Later, fuzzy C-means algorithm was shown to reveal layers similar to well-established histological layers in AC based on FTIR microspectroscopic data of bovine and rabbit AC (54). Similar result was recently found in human AC using K-means clustering (55). These clustering results are likely explained by the varying collagen-to-proteoglycan ratio in the different layers of AC. The fuzzy C-means algorithm also differentiated intact and repaired AC from each other in a rabbit model (56).

Polarized infrared light can be used to detect the orientation of molecular bonds. In AC, the polarized FTIR studies have revealed that the intensities of the amide I, the amide II, and the amide III regions vary strongly when polarization plane of infrared light is altered (19, 57–60), whereas the carbohydrate region shows only weak anisotropy in the radial zone of AC (58, 61). It is known that the transition moments of the amide I and II bonds are qualitatively perpendicular to each other (60). This has been utilized to assess the orientation of the collagen fibrils by calculating the ratio of the amide I to the amide II peaks under

polarized infrared light. A comparison between microscopic magnetic resonance imaging, polarized light microscopy, and polarized FTIR imaging in zonal differentiation of AC was conducted, and criteria were established to obtain comparable results between the techniques (62). Using the polarized light FTIR microscopy, the collagen fibril orientation was shown to differ from healthy cartilage in equine repair cartilage after a full-thickness chondral defect. The results of the study revealed that the orientation of the collagen fibrils was random in all regions except in the superficial layer (25).

Infrared fiber optic probe is a technique that enables spectroscopic measurement of AC during arthroscopy *in situ*. Decrease in the collagen integrity was detected in arthritic human tibial AC as compared to visually normal ones in the first infrared fiber optic probe study (63). Later, infrared fiber optic probe together with PLS model was used to monitor changes in AC surface after ligament transection and medial menisectomy in rabbit (26). Strong correlations have also been obtained between Infrared fiber optic probe data and histological grading of OA using PLS models (51, 64). Furthermore, the clinical outcome of autologous chondrocyte implantation in human AC was shown to correlate with the proteoglycan content and the collagen integrity determined using infrared fiber optic probe (65). Recently, the feasibility of identifying collagen type based on infrared fiber optic measurements was demonstrated, which could be beneficial for monitoring tissue repair (46).

Raman spectroscopy

Raman spectroscopy is based on inelastic scattering of monochromatic light from the sample. Typically, a laser beam of monochromatic light is focused on the sample. A vast majority of the scattered light is elastically scattered (Rayleigh scattering). This is rejected from the detector by a filter that corresponds to the used laser wavelength. The weak, inelastically scattered (Raman scattering) portion of the light is collected and dispersed to the detector by using one or multiple diffraction gratings. In Raman microscopy, a Raman spectroscope is combined with a standard optical microscope. Chemical imaging with a spatial resolution of less than one micrometer can be achieved with a Raman microscope.

Raman spectroscopy does not require extensive sample preparation. In principle, a fresh tissue block can be used for the measurements. On the other hand, fixed samples can also be used, although some spectroscopic alterations are seen due to fixation (15). When measuring thin sections, it is best to place the samples onto, e.g., CaF_2 windows to minimize signal contribution from the material under the sample. A typical Raman spectrum of AC is shown in Figure 1(B), and tentative assignments of the peaks found in the spectrum are shown in Table 2.

The structure of glycosaminoglycans and proteoglycans of AC was investigated by means of Raman microspectroscopy. Spectra of hyaluronan, chondroitin-4-sulfate, chondroitin-6-sulfate, aggrecan monomers, and aggrecan aggregates were presented. Furthermore, it was shown that the Raman spectrum of aggrecan is dominated by chondroitin sulfate (66). The sulfate peak at 1,062 cm^{-1} has been used for evaluating proteoglycan content in AC (67). B-type carbonate, which has a strong Raman band at 1,070 cm^{-1}, partially overlaps with the sulfate peak. Therefore, the CH$_3$ symmetric deformation peak at 1,375 cm^{-1} may be a better choice for glycosaminoglycans if calcified cartilage is included in the analyses (68).

Several univariate parameters were introduced for compositional analysis of AC in a Raman microscopic study. DNA contents were evaluated by the sum of intensities at 1,578

Table 2. Assignments of Raman peaks (69, 79).

Wavenumber (cm^{-1})	Assignment
3,330	N=H stretching (Amide A)
1,670	C=O stretching: alpha-helix (Amide I)
1,606	Phenylalanine, tryptophan
1,557	Amide II
1,450	CH$_2$/CH$_3$ scissoring; collagen and other proteins
1,424	COO$^-$, glycosaminoglycans
1,380	CH$_3$, glycosaminoglycans
1,342	CH, glycosaminoglycans
1,269	NH$_2$ bending: alpha-helix (Amide III)
1,241	NH$_2$ bending: random coil (Amide III)
1,163	Pyranose ring
1,127	Pyranose ring
1,062	SO$_3^-$ stretching of sulfates in glycosaminoglycans
1,033	Phenylalanine
1,002	Phenylalanine
940	C—C deformation of aggrecan / C—O—C stretching of glycosaminoglycans
876	C—C, Hydroxyproline
856	C—C, Proline

cm^{-1}, 1,488 cm^{-1}, and 782 cm^{-1}, chondroitin sulfate by the sum of intensities at 1,380 cm^{-1}, 1,342 cm^{-1}, and 1,068 cm^{-1}, collagen by the sum of the peaks at 1,271 cm^{-1}, 1,246 cm^{-1}, 920 cm^{-1}, 857 cm^{-1}, and 816 cm^{-1}, and non-collagenous proteins (detected upon mapping peaks associated with aromatic amino acids) from the peaks at 1,555 cm^{-1}, 1,127 cm^{-1}, and 1,004 cm^{-1} (69). The peak intensities can be used to visualize the distributions of these components in the tissue (Figure 3).

Extracellular matrix formation by chondrocytes in a medium-throughput culture system can be monitored by Raman microspectroscopy. The peak located at 937 cm^{-1}, assigned to proline/hydroxyproline/C–C skeletal of the collagen backbone, was found to be feasible to assess the collagen formation in chondrocyte pellets (70). Further, the development of AC was studied by applying Raman microspectroscopy to fetal human femur cartilage. HCA effectively separated chondrocytes and ECM based on the Raman spectra. DNA/RNA peak
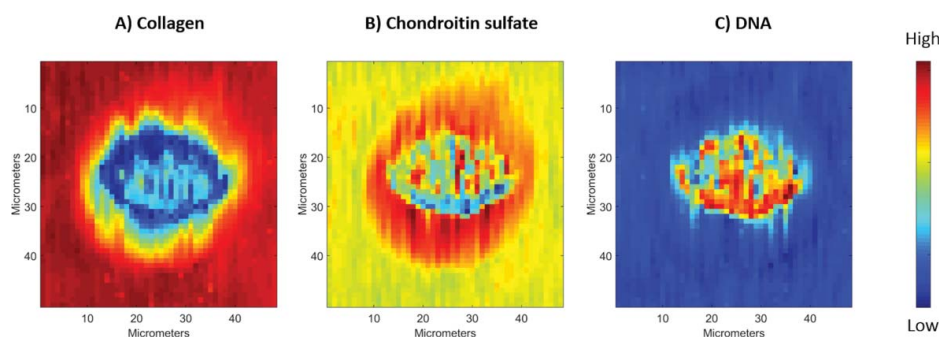
Figure 3. Raman microscopy enables chemical mapping of chondrocytes. The maps above show the distributions of (A) the collagen (the integrated area under the amide I), (B) chondroitin sulfate (the sum of the intensities at 1,061 cm^{-1}, 1,342 cm^{-1}, 1,380 cm^{-1}, and 1,414 cm^{-1}), and (C) DNA (the sum of the intensities at 788 cm^{-1}, 1,488 cm^{-1}, and 1,578 cm^{-1}). The intensities are based on publications by Bonifacio et al. and Ellis et al. (66, 69). The amount of the collagen is high in the ECM. A high amount of chondroitin sulfate produced by the chondrocyte is seen around it, whereas DNA is found inside the chondrocyte.

at 1,576 cm^{-1} seemed to display the most notable difference between the cell spectra and ECM spectra (67).

Stimulated Raman scattering was used for investigating fresh equine AC and subchondral bone. The use of fresh samples enabled the study of lipids in the tissue at the CH vibrational region (2,800–3,000 cm^{-1}). Lipid distributions were visualized by analyzing the peaks at 2,840 cm^{-1} and 2,870 cm^{-1}, and the peak at 2,930 cm^{-1} was used as an indicator for proteins. The mineral content, measured by the carbonate (1,070 cm^{-1}) and the phosphate (959 cm^{-1}) peaks, clearly differentiated non-calcified cartilage from the calcified cartilage (71).

Raman microscopy is well suited for studying chondrocytes and their environment (Figure 3). For this purpose, either the earlier mentioned univariate parameters or different multivariate analysis methods can be applied. Principal component analysis (PCA) has been shown to differentiate the ECM from the chondrocytes. PLS regression models were built for semi-quantitative analysis of DNA, chondroitin sulfate, collagen, and non-collagenous proteins to show their distribution in the chondrocytes and the surrounding ECM. HCA and Fuzzy C-means clustering were used to classify the spectra in unsupervised manner to show the distribution of different biochemical constituents and to reveal the tissue morphology (69).

An alternative way of clustering called "R-mode analysis" was introduced for the analysis of Raman spectroscopic images of AC. Instead of looking at the similarities between the spectra, R-mode analysis compares the univariate images based on different wavenumbers and groups the images with the same pattern of intensity distribution together. A resulting cluster is characterized by a set of Raman shifts and an average image based on these wavenumbers. The technique separated the cell regions, the pericellular region, and the ECM from each other in a similar manner as the traditional multivariate analysis methods (72).

The effects of impact loads on porcine AC were studied by polarized Raman spectroscopy. The most significant differences between the control samples and the impact-loaded samples were seen when the polarizer and the analyzer were parallel to each other. Differences were seen in pyranose ring peak at 1,126 cm^{-1}, which separated control group from impact groups with high sensitivity and specificity. Further, the peak area ratio of proline (856 cm^{-1}) to hydroxyproline (875 cm^{-1}) decreased for impact groups in the parallel-polarized spectra. This may be an indication of damaged collagen helix structure or decrease in proline uptake caused by chondrocyte death after impact (73).

Changes in collagen secondary structure can be assessed by deconvolution of the amide III band. This has been demonstrated in a study where Del1 (+/−) transgenic mice were compared with wild-type mice. Del1 (+/−) mice have a mutation in the COL2A1 gene, which causes a truncation in collagen polypeptide chains. Band ratio of 1,241 cm^{-1} (random coil content) to 1,269 cm^{-1} (alpha-helix content) was used to measure the degree of disorder in the collagen secondary structure (74). In a later study, deconvolution of the amide III band region was also used to assess the differences between healthy control and osteoarthritic human knee tibial plateau samples. The band ratio increased as a function of the OA grading (75).

Raman microspectroscopy was successfully used for identification of chondrocyte differentiation state by characteristic proteoglycan peaks at 1,065 cm^{-1}, 1,079 cm^{-1}, and 1,300 cm^{-1} and by using PCA. Raman spectra of cultured human primary chondrocytes and chondrosarcoma-derived cells were also differentiated by PCA (76). In a recent study, osteoarthritic chondrocytes were isolated from the femoral condyle of patients undergoing

total knee replacement surgery. The chondrocytes were sedimented in a well on a CaF_2 window and covered by a quartz cover slip, and the measurements were conducted using a confocal Raman microscope. PCA was successfully used to associate the chondrocytes to different OA grades (77).

An approach to detect OA in human AC used a combination of different metrics built on pairs of disease modeling materials. A single metric was based on principal component analysis–linear discriminant analysis (PCA–LDA). The models were based on the following pairs: healthy and osteoarthritic human AC, rat AC and rat injury-induced fibrocartilage, and collagens of type I and II. An additional LDA analysis applied to the combination of the two best metrics (human AC and rat AC-based models) resulted in excellent classification in case of human AC spectra of low signal-to-noise ratio (78).

Another study was conducted to detect biomolecular changes in the ECM of AC during OA. Raman imaging revealed that the amount of disordered coil collagen increases significantly in the early OA. A decrease in proteoglycan contents was also observed. A PCA-based classification algorithm was successfully used to classify the samples according to their ICRS scoring. This is a promising result, as PCA is an unsupervised technique, and it is not specifically taught to find OA-related features (79).

NIR spectroscopy (4,000–12,500 cm^{-1})

NIR spectroscopy utilizes shorter wavelengths of electromagnetic spectrum than FTIR (mid-IR) spectroscopy. NIR spectroscopy studies molecular overtone and combination vibrations. These vibrations are often seen as very broad peaks in the measured spectra. Thus, it is difficult to assign an absorption peak to specific chemical component. Therefore, multivariate analysis techniques are often needed for accurate analysis of NIR spectra. The instrumentation in both infrared spectroscopies is quite similar to each other. One obvious advantage of NIR spectroscopy over FTIR and Raman spectroscopies is the high penetration depth of NIR light. It is also possible to measure aqueous samples with NIR spectroscopy. NIR spectroscopy measurements are commonly done in a diffusion reflectance setting. Therefore, it is not easy to localize the origins of the measured signal as diffusion reflectance gives averaged information from multiple depths of the sample. On the other hand, this may be well suited for arthroscopic investigation of, e.g., knee joint to give accurate information about the status of knee cartilage. A typical NIR spectrum of AC is shown in Figure 1(C), and the assignments of the broad absorption peaks found in the spectrum are shown in Table 1.

The penetration depth of NIR light in AC varies from 0.5 mm to at least 5 mm at 4,000–10,000 cm^{-1} wavenumber range. Therefore, a NIR spectrum collected from a typical human cartilage arises from both the cartilage and the subchondral bone underneath it (80, 81). It is possible to measure the thickness of the cartilage with NIR spectroscopy and PLS regression. This has been demonstrated in bovine patellae in a thickness range of 1.2–2.5 mm (82) and in rat AC (83).

The integrated areas of the peaks centered at 5200 cm^{-1} and 6890 cm^{-1} were shown to be associated with the combination of free and bound water, and with free water only, respectively. Furthermore, PLS regression models were successfully used to predict total and free water contents in bovine nasal cartilage (84). In an attempt to obtain the information of FTIR (mid-IR) spectra from NIR spectra, engineered cartilage constructs were measured in transmission mode covering a wavenumber range of 800–6,000 cm^{-1}. Cross-validated PLS

regression models were used to predict the mid-IR collagen peaks (amide I, amide II, and 1338 cm^{-1}) and the proteoglycan peak (850 cm^{-1}) from the NIR region. First derivative spectra and multiplicative scattering correction were used as preprocessing methods. The predictive performance of the models for the amide I, the amide II, and the proteoglycan peaks were excellent ($R^2 > 0.9$), indicating the capabilities of multivariate models to extract accurate information from overlapping spectra (22).

NIR spectroscopy can also reveal mechanical properties of AC. NIR spectroscopy was used to investigate AC reswelling after compression. A PLS regression model successfully predicted the reswelling of intact and enzymatically degraded bovine AC (85). Spatial mapping of proteoglycan content in AC has been conducted by creating a calibration sample set of AC samples with different total amounts of proteoglycan. This was achieved by enzymatic degradation of proteoglycans. A PLS regression model built with the calibration samples was applied to the spectroscopic mapping data of a bovine patella with a focal defect. The analysis revealed a loss of proteoglycans in the focal defect area (86). In another study based on enzymatic degradation of the ECM, multivariate modeling of NIR spectra was used to distinguish normal and enzymatically degraded bovine patellae. Trypsin was used to obtain almost complete depletion of proteoglycans from the cartilage tissue. Higher overall absorbance was observed in the enzymatically degraded cartilage due to higher water content. Otherwise, the average spectra were very similar to each other. The best classification accuracy was obtained by using a PLS regression model after first-derivative pre-processing method (87).

In a subsequent study, a more realistic setting regarding OA was investigated by collecting normal bovine patellae and bovine patellae with focal OA. A discriminant analysis function was built based on clearly identifiable NIR absorption peaks in raw and 2nd derivative spectra. The function distinguished the normal cartilage from degraded tissue with greater than 95% accuracy (88). Potential of NIR spectroscopy for recognizing cartilage degradation in a rat OA model has also been studied. Three different methods, menisectomy, anterior cruciate ligament transection, and intra-articular injection of mono-ido-acetate, were used to induce different severity of OA. An excellent correlation between NIR spectra and Mankin score OA grading was achieved by using PLS regression (83). Further, different components of Mankin score were successfully predicted using separate PLS regression models (89).

PLS regression models were also used to predict proteoglycan and collagen contents in human AC of total knee replacement patients. Grade of cartilage lesion was also predicted. In general, the results were not as good as in animal models obtained earlier (90). However, better results were obtained in a later *in vitro* NIR spectroscopic study of human AC focusing on biochemical, biomechanical, and histological properties of the tissue. The sample material of the study comprised of osteochondral plugs from tibia and femur. The study demonstrated that the uronic acid content, water content, dynamic modulus, equilibrium modulus, Mankin score, and thickness of AC can all be predicted from NIR spectra using PLS regression models, and that NIR-based evaluation could be used for rapid assessment of tissue integrity (91).

The first NIR arthroscopic study of AC calculated the ratio of the 1st OH and CH combination overtones (1,430 nm–1,475 nm, $\sim$ 6,780–6,990 cm^{-1}) and the 2nd CH overtone (1,150 nm–1,220 nm, $\sim$ 8,195–8,695 cm^{-1}) to evaluate the relative proportion of water to organic substances. The water content was shown to be significantly higher in cartilage lesions than in intact cartilage (92). Later, the same absorbance ratio was shown to correlate with Mankin score, water content, and mechanical stiffness in sheep femoral condyle

cartilage in an *in vitro* study (93). The water peak ratio also correlated with Knee Injury and Osteoarthritis Outcome Score (KOOS) sub-parameters in a clinical knee pain study, but the correlations were only weak ($r \le 0.3$) (94). Linear combination of the water peaks was shown to correlate negatively with the degree of degeneration, and positively with Young's modulus in human AC (95). A commercial NIR spectroscopic arthroscopic probe has been introduced based on the aforementioned studies. The probe gives a semi-quantitative value between 0 and 100 that represents the cartilage quality (96–98).

NIR spectroscopy has been recently demonstrated to be a feasible method for assessing the composition of engineered cartilage in a non-destructive manner. PLS regression models were successfully used to measure water, proteoglycan, and collagen contents in engineered cartilage. The information may be utilized when determining the optimal time to harvest the engineered tissue for clinical purposes (99).

Summary

Vibrational spectroscopic techniques have been widely used to assess the biochemical composition, biomechanical properties, and quality of AC. The techniques can be seen as complementary to each other. The spectroscopic methods offer means for chemical imaging of unstained histological sections, rapid non-destructive evaluation of samples *in vitro*, and evaluation of cartilage quality *in vivo* during arthroscopy. FTIR imaging is best suited for chemical imaging of large areas from unstained histological sections due to its speed advantage over Raman imaging. Importantly, quantitative analysis is feasible using FTIR imaging as the thickness of histological sections is known, and, therefore, the volume of the material the infrared light transmits through is the same between the samples. Raman spectroscopic imaging is also often conducted from histological sections. Compared to FTIR, the major advantage of Raman spectroscopy over FTIR spectroscopy is that no sample preparation is necessary, and it is also well suited for measuring samples that contain water. Thus, Raman spectroscopic imaging can be conducted easily also in physiological conditions. It is also possible to image single chondrocytes with sub-micron resolution available with Raman microscopy. However, quantitative analysis is more challenging due to multiple factors affecting the measurement outcome. In NIR spectroscopy, it is difficult to pinpoint the exact volume where the NIR spectrum is collected in a diffuse reflectance setting. NIR spectrum gives an overall spectroscopic signal of AC, which can be beneficial in arthroscopic evaluation of AC condition. Even though NIR spectra display mainly very broad peaks, multivariate regression models are able to extract accurate information about the bulk composition and properties of AC from the spectra.

Acknowledgments

Funding

References

1. Huber, M., Trattnig, S., and Lintner, F. (2000) Anatomy, biochemistry, and physiology of articular cartilage. *Invest. Radiol.* 35 (10): 573–580.
2. Buckwalter, J. A., Mankin, H. J., and Grodzinsky, A. J. (2005) Articular cartilage and osteoarthritis. *Instr. Course Lect.* 54: 465–480.
3. Xia, Y., Moody, J. B., Burton-Wurster, N., and Lust, G. (2001) Quantitative in situ correlation between microscopic MRI and polarized light microscopy studies of articular cartilage. *Osteoarthritis Cartilage.* 9 (5): 393–406.
4. Mow, V. C., Ratcliffe, A., and Poole, A. R. (1992) Cartilage and diarthrodial joints as paradigms for hierarchical materials and structures. *Biomaterials* 13 (2): 67–97.
5. Schmidt, M. B., Mow, V. C., Chun, L. E., and Eyre, D. R. (1990) Effects of proteoglycan extraction on the tensile behavior of articular cartilage. *J. Orthop. Res.* 8 (3): 353–363.
6. Venn, M., and Maroudas, A. (1977) Chemical composition and swelling of normal and osteoarthrotic femoral head cartilage. I. Chemical composition. *Ann. Rheum. Dis.* 36 (2): 121–129.
7. Maroudas, A., and Venn, M. (1977) Chemical composition and swelling of normal and osteoarthrotic femoral head cartilage. II. Swelling. *Ann. Rheum. Dis.* 36 (5): 399–406.
8. Guilak, F., Ratcliffe, A., Lane, N., Rosenwasser, M. P., and Mow, V. C. (1994) Mechanical and biochemical changes in the superficial zone of articular cartilage in canine experimental osteoarthritis. *J. Orthop. Res.* 12 (4): 474–484.
9. Panula, H. E., Hyttinen, M. M., Arokoski, J. P., Langsjo, T. K., Pelttari, A., Kiviranta, I., and Helminen, H. J. (1998) Articular cartilage superficial zone collagen birefringence reduced and cartilage thickness increased before surface fibrillation in experimental osteoarthritis. *Ann. Rheum. Dis.* 57 (4): 237–245.
10. Hunziker, E. B. (2002) Articular cartilage repair: Basic science and clinical progress. A review of the current status and prospects. *Osteoarthritis Cartilage* 10 (6): 432–463.
11. Lasch, P., and Naumann, D. (2006) Spatial resolution in infrared microspectroscopic imaging of tissues. *Biochim. Biophys. Acta.* 1758 (7): 814–829.
12. Hanifi, A., McGoverin, C., Ou, Y. T., Safadi, F., Spencer, R. G., and Pleshko, N. (2013) Differences in infrared spectroscopic data of connective tissues in transflectance and transmittance modes. *Anal. Chim. Acta.* 779: 41–49.
13. Filik, J., Frogley, M. D., Pijanka, J. K., Wehbe, K., and Cinque, G. (2012) Electric field standing wave artefacts in FTIR micro-spectroscopy of biological materials. *Analyst.* 137 (4): 853–861.
14. Spencer, R. G., Calton, E. F., and Camacho, N. P. (2006) Statistical comparison of Fourier transform infrared spectra. *J. Biomed. Opt.* 11 (6): 064023.
15. Faolain, E. O., Hunter, M. B., Byrne, J. M., Kelehan, P., Lambkin, H. A., Byrne, H. J., and Lyng, F. M. (2005) Raman spectroscopic evaluation of efficacy of current paraffin wax section dewaxing agents. *J. Histochem. Cytochem.* 53 (1): 121–129.
16. Ly, E., Piot, O., Wolthuis, R., Durlach, A., Bernard, P., and Manfait, M. (2008) Combination of FTIR spectral imaging and chemometrics for tumour detection from paraffin-embedded biopsies. *Analyst.* 133 (2): 197–205.
17. Rieppo, J., Hyttinen, M. M., Jurvelin, J. S., and Helminen, H. J. (2004) Reference sample method reduces the error caused by variable cryosection thickness in Fourier transform infrared imaging. *Appl. Spectrosc.* 58 (1): 137–140.
18. Kiraly, K., Hyttinen, M. M., Lapvetelainen, T., Elo, M., Kiviranta, I., Dobai, J., Modis, L., Helminen, H. J., and Arokoski, J. P. (1997) Specimen preparation and quantification of collagen birefringence in unstained sections of articular cartilage using image analysis and polarizing light microscopy. *Histochem. J.* 29 (4): 317–327.
19. Camacho, N. P., West, P., Torzilli, P. A., and Mendelsohn, R. (2001) FTIR microscopic imaging of collagen and proteoglycan in bovine cartilage. *Biopolymers* 62 (1): 1–8.
20. Potter, K., Kidder, L. H., Levin, I. W., Lewis, E. N., and Spencer, R. G. (2001) Imaging of collagen and proteoglycan in cartilage sections using Fourier transform infrared spectral imaging. *Arthritis Rheum.* 44 (4): 846–855.

21. Kim, M., Bi, X., Horton, W. E., Spencer, R. G., and Camacho, N. P. (2005) Fourier transform infrared imaging spectroscopic analysis of tissue engineered cartilage: histologic and biochemical correlations. *J. Biomed. Opt.* 10 (3): 031105.

22. Baykal, D., Irrechukwu, O., Lin, P. C., Fritton, K., Spencer, R. G., and Pleshko, N. (2010) Nondestructive assessment of engineered cartilage constructs using near-infrared spectroscopy. *Appl. Spectrosc.* 64 (10): 1160–1166.

23. West, P. A., Torzilli, P. A., Chen, C., Lin, P., and Camacho, N. P. (2005) Fourier transform infrared imaging spectroscopy analysis of collagenase-induced cartilage degradation. *J. Biomed. Opt.* 10 (1): 14015.

24. David-Vaudey, E., Burghardt, A., Keshari, K., Brouchet, A., Ries, M., and Majumdar, S. (2005) Fourier transform infrared imaging of focal lesions in human osteoarthritic cartilage. *Eur. Cell. Mater.* 10: 51–60.

25. Bi, X., Yang, X., Bostrom, M. P., and Camacho, N. P. (2006) Fourier transform infrared imaging spectroscopy investigations in the pathogenesis and repair of cartilage. *Biochim. Biophys. Acta.* 1758 (7): 934–941.

26. Bi, X., Yang, X., Bostrom, M. P., Bartusik, D., Ramaswamy, S., Fishbein, K. W., Spencer, R. G., and Camacho, N. P. (2007) Fourier transform infrared imaging and MR microscopy studies detect compositional and structural changes in cartilage in a rabbit model of osteoarthritis. *Anal. Bioanal Chem.* 387 (5): 1601–1612.

27. Saarakkala, S., Julkunen, P., Kiviranta, P., Mäkitalo, J., Jurvelin, J. S., and Korhonen, R. K. (2010) Depth-wise progression of osteoarthritis in human articular cartilage: investigation of composition, structure and biomechanics. *Osteoarthritis Cartilage.* 18 (1): 73–81.

28. Reiter, D. A., Roque, R. A., Lin, P. C., Irrechukwu, O., Doty, S., Longo, D. L., Pleshko, N., and Spencer, R. G. (2011) Mapping proteoglycan-bound water in cartilage: Improved specificity of matrix assessment using multiexponential transverse relaxation analysis. *Magn. Reson. Med.* 65 (2): 377–384.

29. Saadat, E., Lan, H., Majumdar, S., Rempel, D. M., and King, K. B. (2006) Long-term cyclical in vivo loading increases cartilage proteoglycan content in a spatially specific manner: an infrared microspectroscopic imaging and polarized light microscopy study. *Arthritis Res. Ther.* 8 (5): R147.

30. Crombie, D. E., Turer, M., Zuasti, B. B., Wood, B., McNaughton, D., Nandakumar, K. S., Holmdahl, R., Van Damme, M. P., and Rowley, M. J. (2005) Destructive effects of murine arthritogenic antibodies to type II collagen on cartilage explants in vitro. *Arthritis Res. Ther.* 7 (5): R927–37.

31. Mahmoodian, R., Leasure, J., Philip, P., Pleshko, N., Capaldi, F., and Siegler, S. (2011) Changes in mechanics and composition of human talar cartilage anlagen during fetal development. *Osteoarthritis Cartilage.* 19 (10): 1199–1209.

32. Turunen, S. M., Lammi, M. J., Saarakkala, S., Koistinen, A., and Korhonen, R. K. (2012) Hypotonic challenge modulates cell volumes differently in the superficial zone of intact articular cartilage and cartilage explant. *Biomech. Model. Mechanobiol.* 11 (5): 665–675.

33. Saarakkala, S., and Julkunen, P. (2010) Specificity of Fourier transform infrared (FTIR) microspectroscopy to estimate depth-wise proteoglycan content in normal and osteoarthritic human articular cartilage. *Cartilage* 1 (4): 262–269.

34. Laasanen, M. S., Saarakkala, S., Toyras, J., Rieppo, J., and Jurvelin, J. S. (2005) Site-specific ultrasound reflection properties and superficial collagen content of bovine knee articular cartilage. *Phys. Med. Biol.* 50 (14): 3221–3233.

35. Rieppo, J., Hyttinen, M. M., Halmesmaki, E., Ruotsalainen, H., Vasara, A., Kiviranta, I., Jurvelin, J. S., and Helminen, H. J. (2009) Changes in spatial collagen content and collagen network architecture in porcine articular cartilage during growth and maturation. *Osteoarthritis Cartilage* 17 (4): 448–455.

36. Brama, P. A., Holopainen, J., van Weeren, P. R., Firth, E. C., Helminen, H. J., and Hyttinen, M. M. (2009) Influence of exercise and joint topography on depth-related spatial distribution of proteoglycan and collagen content in immature equine articular cartilage. *Equine Vet. J.* 41 (6): 557–563.

37. Jiang, E. Y., and Rieppo, J. (2006) Enhancing FTIR imaging capabilities with two-dimensional correlation spectroscopy (2DCOS): A study of concentration gradients of collagen and proteoglycans in human patellar cartilage. *J. Mol. Struct.* 799 (1–3): 196–203.

38. Rieppo, L., Saarakkala, S., Narhi, T., Holopainen, J., Lammi, M., Helminen, H. J., Jurvelin, J. S., and Rieppo, J. (2010) Quantitative analysis of spatial proteoglycan content in articular cartilage with Fourier transform infrared imaging spectroscopy: Critical evaluation of analysis methods and specificity of the parameters. *Microsc. Res. Tech.* 73 (5): 503–512.

39. Rieppo, L., Saarakkala, S., Narhi, T., Helminen, H. J., Jurvelin, J. S., and Rieppo, J. (2012) Application of second derivative spectroscopy for increasing molecular specificity of Fourier transform infrared spectroscopic imaging of articular cartilage. *Osteoarthritis Cartilage* 20 (5): 451–459.

40. Rieppo, L., Narhi, T., Helminen, H. J., Jurvelin, J. S., Saarakkala, S., and Rieppo, J. (2013) Infrared spectroscopic analysis of human and bovine articular cartilage proteoglycans using carbohydrate peak or its second derivative. *J. Biomed. Opt.* 18 (9): 097006.

41. Yin, J., and Xia, Y. (2010) Macromolecular concentrations in bovine nasal cartilage by Fourier transform infrared imaging and principal component regression. *Appl. Spectrosc.* 64 (11): 1199–1208.

42. Yin, J., Xia, Y., and Lu, M. (2012) Concentration profiles of collagen and proteoglycan in articular cartilage by Fourier transform infrared imaging and principal component regression. *Spectrochim. Acta A Mol. Biomol. Spectrosc.* 88: 90–96.

43. Yin, J., and Xia, Y. (2014) Proteoglycan concentrations in healthy and diseased articular cartilage by Fourier transform infrared imaging and principal component regression. *Spectrochim. Acta A Mol. Biomol. Spectrosc.* 133: 825–830.

44. Rieppo, L., Rieppo, J., Jurvelin, J. S., and Saarakkala, S. (2012) Fourier transform infrared spectroscopic imaging and multivariate regression for prediction of proteoglycan content of articular cartilage. *PLoS One* 7 (2): e32344.

45. Rieppo, L., Saarakkala, S., Jurvelin, J. S., and Rieppo, J. (2014) Optimal variable selection for Fourier transform infrared spectroscopic analysis of articular cartilage composition. *J. Biomed. Opt.* 19 (2): 027003.

46. Hanifi, A., McCarthy, H., Roberts, S., and Pleshko, N. (2013) Fourier transform infrared imaging and infrared fiber optic probe spectroscopy identify collagen type in connective tissues. *PLoS One* 8 (5): e64822.

47. Rieppo, L., Saarakkala, S., Jurvelin, J. S., and Rieppo, J. (2013) Prediction of compressive stiffness of articular cartilage using Fourier transform infrared spectroscopy. *J. Biomech.* 46 (7): 1269–1275.

48. Paschalis, E. P., Verdelis, K., Doty, S. B., Boskey, A. L., Mendelsohn, R., and Yamauchi, M. (2001) Spectroscopic characterization of collagen cross-links in bone. *J. Bone Miner. Res.* 16 (10): 1821–1828.

49. Kim, M., Kraft, J. J., Volk, A. C., Pugarelli, J., Pleshko, N., and Dodge, G. R. (2011) Characterization of a cartilage-like engineered biomass using a self-aggregating suspension culture model: molecular composition using FT-IRIS. *J. Orthop. Res.* 29 (12): 1881–1887.

50. Masahiko, T., Damle, S., Penmatsa, M., West, P., Yang, X., Bostrom, M., Hidaka, C., Yamauchi, M., and Pleshko, N. (2012) Temporal changes in collagen cross-links in spontaneous articular cartilage repair. *Cartilage* 3 (3): 278–287.

51. Hanifi, A., Bi, X., Yang, X., Kavukcuoglu, B., Lin, P. C., DiCarlo, E., Spencer, R. G., Bostrom, M. P., and Pleshko, N. (2012) Infrared fiber optic probe evaluation of degenerative cartilage correlates to histological grading. *Am. J. Sports Med.* 40 (12): 2853–2861.

52. Croxford, A. M., Crombie, D., McNaughton, D., Holmdahl, R., Nandakumar, K. S., and Rowley, M. J. (2010) Specific antibody protection of the extracellular cartilage matrix against collagen antibody-induced damage. *Arthritis Rheum.* 62 (11): 3374–3384.

53. Croxford, A. M., Nandakumar, K. S., Holmdahl, R., Tobin, M. J., McNaughton, D., and Rowley, M. J. (2011) Chemical changes demonstrated in cartilage by synchrotron infrared microspectroscopy in an antibody-induced murine model of rheumatoid arthritis. *J. Biomed. Opt.* 16 (6): 066004.

54. Kobrina, Y., Rieppo, L., Saarakkala, S., Jurvelin, J. S., and Isaksson, H. (2012) Clustering of infrared spectra reveals histological zones in intact articular cartilage. *Osteoarthritis Cartilage* 20 (5): 460–468.

55. Oinas, J., Rieppo, L., Finnila, M. A., Valkealahti, M., Lehenkari, P., and Saarakkala, S. (2016) Imaging of osteoarthritic human articular cartilage using fourier transform infrared microspectroscopy combined with multivariate and univariate analysis. *Sci. Rep.* 6: 30008.

56. Kobrina, Y., Rieppo, L., Saarakkala, S., Pulkkinen, H. J., Tiitu, V., Valonen, P., Kiviranta, I., Jurvelin, J. S., and Isaksson, H. (2013) Cluster analysis of infrared spectra can differentiate intact and repaired articular cartilage. *Osteoarthritis Cartilage* 21 (3): 462–469.

57. Ramakrishnan, N., Xia, Y., and Bidthanapally, A. (2007) Polarized IR microscopic imaging of articular cartilage. *Phys. Med. Biol.* 52 (15): 4601–4614.

58. Xia, Y., Ramakrishnan, N., and Bidthanapally, A. (2007) The depth-dependent anisotropy of articular cartilage by Fourier-transform infrared imaging (FTIRI). *Osteoarthritis Cartilage* 15 (7): 780–788.

59. Xia, Y., Alhadlaq, H., Ramakrishnan, N., Bidthanapally, A., Badar, F., and Lu, M. (2008) Molecular and morphological adaptations in compressed articular cartilage by polarized light microscopy and Fourier-transform infrared imaging. *J. Struct. Biol.* 164 (1): 88–95.

60. Bi, X., Li, G., Doty, S. B., and Camacho, N. P. (2005) A novel method for determination of collagen orientation in cartilage by Fourier transform infrared imaging spectroscopy (FT-IRIS). *Osteoarthritis Cartilage* 13 (12): 1050–1058.

61. Xia, Y., Mittelstaedt, D., Ramakrishnan, N., Szarko, M., and Bidthanapally, A. (2011) Depth-dependent anisotropies of amides and sugar in perpendicular and parallel sections of articular cartilage by Fourier transform infrared imaging. *Microsc. Res. Tech.* 74 (2): 122–132.

62. Lee, J. H., and Xia, Y. (2013) Quantitative zonal differentiation of articular cartilage by microscopic magnetic resonance imaging, polarized light microscopy, and Fourier-transform infrared imaging. *Microsc. Res. Tech.* 76 (6): 625–632.

63. West, P. A., Bostrom, M. P., Torzilli, P. A., and Camacho, N. P. (2004) Fourier transform infrared spectral analysis of degenerative cartilage: an infrared fiber optic probe and imaging study. *Appl. Spectrosc.* 58 (4): 376–381.

64. Li, G., Thomson, M., Dicarlo, E., Yang, X., Nestor, B., Bostrom, M. P., and Camacho, N. P. (2005) A chemometric analysis for evaluation of early-stage cartilage degradation by infrared fiber-optic probe spectroscopy. *Appl. Spectrosc.* 59 (12): 1527–1533.

65. Hanifi, A., Richardson, J. B., Kuiper, J. H., Roberts, S., and Pleshko, N. (2012) Clinical outcome of autologous chondrocyte implantation is correlated with infrared spectroscopic imaging-derived parameters. *Osteoarthritis Cartilage* 20 (9): 988–996.

66. Ellis, R., Green, E., and Winlove, C. P. (2009) Structural analysis of glycosaminoglycans and proteoglycans by means of Raman microspectrometry. *Connect. Tissue Res.* 50 (1): 29–36.

67. Kunstar, A., Leijten, J., van Leuveren, S., Hilderink, J., Otto, C., van Blitterswijk, C. A., Karperien, M., and van Apeldoorn, A. A. (2012) Recognizing different tissues in human fetal femur cartilage by label-free Raman microspectroscopy. *J. Biomed. Opt.* 17 (11): 116012.

68. Gamsjaeger, S., Klaushofer, K., and Paschalis, E. P. (2014) Raman analysis of proteoglycans simultaneously in bone and cartilage. *J. Raman Spectrosc.* 45 (9): 794–800.

69. Bonifacio, A., Beleites, C., Vittur, F., Marsich, E., Semeraro, S., Paoletti, S., and Sergo, V. (2010) Chemical imaging of articular cartilage sections with Raman mapping, employing uni- and multivariate methods for data analysis. *Analyst.* 135 (12): 3193–3204.

70. Kunstar, A., Otto, C., Karperien, M., van Blitterswijk, C., and van Apeldoorn, A. (2011) Raman microspectroscopy: a noninvasive analysis tool for monitoring of collagen-containing extracellular matrix formation in a medium-throughput culture system. *Tissue Eng. Part C. Methods* 17 (7): 737–744.

71. Mansfield, J., Moger, J., Green, E., Moger, C., and Winlove, C. P. (2013) Chemically specific imaging and in-situ chemical analysis of articular cartilage with stimulated Raman scattering. *J. Biophotonics* 6 (10): 803–814.

72. Bonifacio, A., Beleites, C., and Sergo, V. (2015) Application of R-mode analysis to Raman maps: a different way of looking at vibrational hyperspectral data. *Anal. Bioanal Chem.* 407 (4): 1089–1095.

73. Lim, N. S., Hamed, Z., Yeow, C. H., Chan, C., and Huang, Z. (2011) Early detection of biomolecular changes in disrupted porcine cartilage using polarized Raman spectroscopy. *J. Biomed. Opt.* 16 (1): 017003.

74. Dehring, K. A., Smukler, A. R., Roessler, B. J., and Morris, M. D. (2006) Correlating changes in collagen secondary structure with aging and defective type II collagen by Raman spectroscopy. *Appl. Spectrosc.* 60 (4): 366–372.

75. Takahashi, Y., Sugano, N., Takao, M., Sakai, T., Nishii, T., and Pezzotti, G. (2014) Raman spectroscopy investigation of load-assisted microstructural alterations in human knee cartilage: Preliminary study into diagnostic potential for osteoarthritis. *J. Mech. Behav. Biomed. Mater.* 31: 77–85.

76. Pudlas, M., Brauchle, E., Klein, T. J., Hutmacher, D. W., and Schenke-Layland, K. (2013) Non-invasive identification of proteoglycans and chondrocyte differentiation state by Raman microspectroscopy. *J. Biophotonics* 6 (2): 205–211.

77. Kumar, R., Singh, G. P., Gronhaug, K. M., Afseth, N. K., de Lange Davies, C., Drogset, J. O., and Lilledahl, M. B. (2015) Single cell confocal Raman spectroscopy of human osteoarthritic chondrocytes: a preliminary study. *Int. J. Mol. Sci.* 16 (5): 9341–9353.

78. Richardson, W., Wilkinson, D., Wu, L., Petrigliano, F., Dunn, B., and Evseenko, D. (2014) Ensemble multivariate analysis to improve identification of articular cartilage disease in noisy Raman spectra. *J. Biophotonics* 9999 (9999): 10.1002/jbio.201300200.

79. Kumar, R., Gronhaug, K. M., Afseth, N. K., Isaksen, V., de Lange Davies, C., Drogset, J. O., and Lilledahl, M. B. (2015) Optical investigation of osteoarthritic human cartilage (ICRS grade) by confocal Raman spectroscopy: a pilot study. *Anal. Bioanal Chem.* 407 (26): 8067–8077.

80. McGoverin, C. M., Lewis, K., Yang, X., Bostrom, M. P., and Pleshko, N. (2014) The contribution of bone and cartilage to the near-infrared spectrum of osteochondral tissue. *Appl. Spectrosc.* 68 (10): 1168–1175.

81. Padalkar, M. V., and Pleshko, N. (2015) Wavelength-dependent penetration depth of near infrared radiation into cartilage. *Analyst.* 140 (7): 2093–2100.

82. Afara, I., Singh, S., and Oloyede, A. (2013) Application of near infrared (NIR) spectroscopy for determining the thickness of articular cartilage. *Med. Eng. Phys.* 35 (1): 88–95.

83. Afara, I., Prasadam, I., Crawford, R., Xiao, Y., and Oloyede, A. (2012) Non-destructive evaluation of articular cartilage defects using near-infrared (NIR) spectroscopy in osteoarthritic rat models and its direct relation to Mankin score. *Osteoarthritis Cartilage* 20 (11): 1367–1373.

84. Padalkar, M. V., Spencer, R. G., and Pleshko, N. (2013) Near infrared spectroscopic evaluation of water in hyaline cartilage. *Ann. Biomed. Eng.* 41 (11): 2426–2436.

85. Afara, I.O., Singh, S., and Oloyede, A. (2013) Load-unloading response of intact and artificially degraded articular cartilage correlated with near infrared (NIR) absorption spectra. *J. Mech. Behav. Biomed. Mater.* 20: 249–258.

86. Afara, I. O., Moody, H., Singh, S., Prasadam, I., and Oloyede, A. (2014) Spatial mapping of proteoglycan content in articular cartilage using near-infrared (NIR) spectroscopy. *Biomed. Opt. Express* 6 (1): 144–154.

87. Brown, C. P., Bowden, J. C., Rintoul, L., Meder, R., Oloyede, A., and Crawford, R. W. (2009) Diffuse reflectance near infrared spectroscopy can distinguish normal from enzymatically digested cartilage. *Phys. Med. Biol.* 54 (18): 5579–5594.

88. Brown, C. P., Jayadev, C., Glyn-Jones, S., Carr, A. J., Murray, D. W., Price, A. J., and Gill, H. S. (2011) Characterization of early stage cartilage degradation using diffuse reflectance near infrared spectroscopy. *Phys. Med. Biol.* 56 (7): 2299–2307.

89. Afara, I. O., Prasadam, I., Moody, H., Crawford, R., Xiao, Y., and Oloyede, A. (2014) Near infrared spectroscopy for rapid determination of Mankin score components: a potential tool for quantitative characterization of articular cartilage at surgery. *Arthroscopy* 30 (9): 1146–1155.

90. Stumpfe, S. T., Pester, J. K., Steinert, S., Marintschev, I., Plettenberg, H., Aurich, M., and Hofmann, G. O. (2013) Is there a correlation between biophotonical, biochemical, histological, and visual changes in the cartilage of osteoarthritic knee-joints? *Muscles Ligaments Tendons J.* 3 (3): 157–165.

91. Afara, I. O., Hauta-Kasari, M., Jurvelin, J. S., Oloyede, A., and Toyras, J. (2015) Optical absorption spectra of human articular cartilage correlate with biomechanical properties, histological score and biochemical composition. *Physiol. Meas.* 36 (9): 1913–1928.
92. Spahn, G., Plettenberg, H., Kahl, E., Klinger, H. M., Muckley, T., and Hofmann, G. O. (2007) Near-infrared (NIR) spectroscopy. A new method for arthroscopic evaluation of low grade degenerated cartilage lesions. Results of a pilot study. *BMC Musculoskelet. Disord.* 8: 47.
93. Spahn, G., Plettenberg, H., Nagel, H., Kahl, E., Klinger, H. M., Muckley, T., Gunther, M., Hofmann, G. O., and Mollenhauer, J. A. (2008) Evaluation of cartilage defects with near-infrared spectroscopy (NIR): an ex vivo study. *Med. Eng. Phys.* 30 (3): 285–292.
94. Hofmann, G. O., Marticke, J., Grossstuck, R., Hoffmann, M., Lange, M., Plettenberg, H. K., Braunschweig, R., Schilling, O., Kaden, I., and Spahn, G. (2010) Detection and evaluation of initial cartilage pathology in man: A comparison between MRT, arthroscopy and near-infrared spectroscopy (NIR) in their relation to initial knee pain. *Pathophysiology.* 17 (1): 1–8.
95. Marticke, J. K., Hosselbarth, A., Hoffmeier, K. L., Marintschev, I., Otto, S., Lange, M., Plettenberg, H. K., Spahn, G., and Hofmann, G. O. (2010) How do visual, spectroscopic and biomechanical changes of cartilage correlate in osteoarthritic knee joints? *Clin. Biomech. (Bristol, Avon).* 25 (4): 332–340.
96. Spahn, G., Klinger, H. M., Baums, M., Hoffmann, M., Plettenberg, H., Kroker, A., and Hofmann, G. O. (2010) Near-infrared spectroscopy for arthroscopic evaluation of cartilage lesions: Results of a blinded, prospective, interobserver study. *Am. J. Sports Med.* 38 (12): 2516–2521.
97. Spahn, G., Felmet, G., and Hofmann, G. O. (2013) Traumatic and degenerative cartilage lesions: arthroscopic differentiation using near-infrared spectroscopy (NIRS). *Arch. Orthop. Trauma. Surg.* 133 (7): 997–1002.
98. Guenther, D., Liu, C., Horstmann, H., Krettek, C., Jagodzinski, M., and Haasper, C. (2014) Near-infrared spectroscopy correlates with established histological scores in a miniature pig model of cartilage regeneration. *Open Orthop. J.* 8: 93–99.
99. McGoverin, C. M., Hanifi, A., Palukuru, U. P., Yousefi, F., Glenn, P. B., Shockley, M., Spencer, R. G., and Pleshko, N. (2016) Nondestructive assessment of engineered cartilage composition by near infrared spectroscopy. *Ann. Biomed. Eng.* 44 (3): 680–692.